Analytical collapse models and nonlinear probability distribution function

Tsz Yan Lam

University of Pennsylvania

Nov 11, 2008
UC Berkeley

Outline

Introduction

Spherical Collapse and real space PDF

Ellipsoidal Collapse and zspace PDF

Large Scale Structure with non-Gaussianity

Introduction

- Current constraints:

$\Omega_b h^2$	$0.02267^{+0.00058}_{-0.00059}$
$\Omega_c h^2$	0.1131 ± 0.0034
Ω_Λ	0.726 ± 0.015
σ_8	0.812 ± 0.016
H_0	70.5 ± 1.3
n_s	0.960 ± 0.013

Introduction

- Current constraints:

$\Omega_b h^2$	$0.02267^{+0.00058}_{-0.00059}$
$\Omega_c h^2$	0.1131 ± 0.0034
Ω_Λ	0.726 ± 0.015
σ_8	0.812 ± 0.016
H_0	70.5 ± 1.3
n_s	0.960 ± 0.013

- The next generation of sky surveys (DES, PanStarrs, JDEM, LSST) aims to constrain cosmological models in percent-level precision.

Introduction

- Current constraints:

$\Omega_b h^2$	$0.02267^{+0.00058}_{-0.00059}$
$\Omega_c h^2$	0.1131 ± 0.0034
Ω_Λ	0.726 ± 0.015
σ_8	0.812 ± 0.016
H_0	70.5 ± 1.3
n_s	0.960 ± 0.013

- The next generation of sky surveys (DES, PanStarrs, JDEM, LSST) aims to constrain cosmological models in percent-level precision.
- Need to understand how gravity has affected the observed signals.

Introduction

- Current constraints:

$\Omega_b h^2$	$0.02267^{+0.00058}_{-0.00059}$
$\Omega_c h^2$	0.1131 ± 0.0034
Ω_Λ	0.726 ± 0.015
σ_8	0.812 ± 0.016
H_0	70.5 ± 1.3
n_s	0.960 ± 0.013

- The next generation of sky surveys (DES, PanStarrs, JDEM, LSST) aims to constrain cosmological models in percent-level precision.
- Need to understand how gravity has affected the observed signals.
- My work: study of large scale structure formation and its implications for cosmological measurements.

Introduction

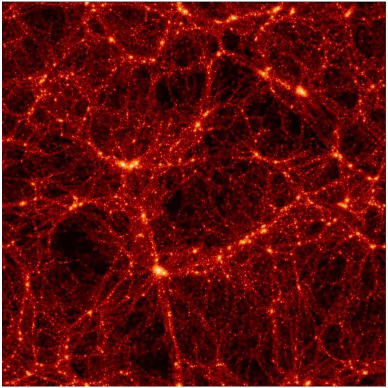

- Study of the PDF of dark matter field;

Introduction

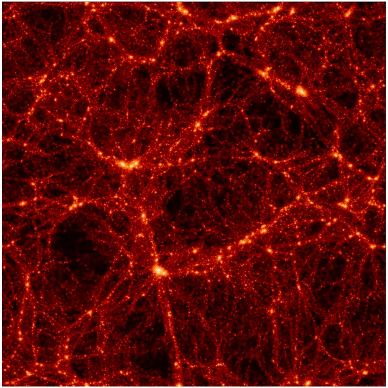

- Study of the PDF of dark matter field;
- Analytical collapse models to describe the evolution of overdensity;

Introduction

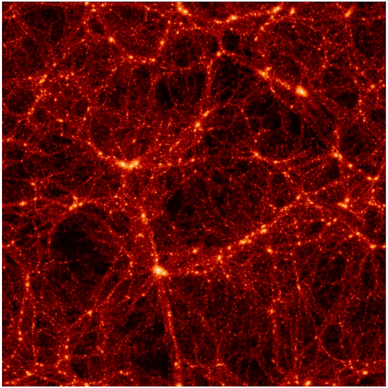

- Study of the PDF of dark matter field;
- Analytical collapse models to describe the evolution of overdensity;
- Spherical Collapse Model (real space); Ellipsoidal Collapse Model (redshift space)

Outline

Introduction

Spherical Collapse and real space PDF

Ellipsoidal Collapse and zspace PDF

Large Scale Structure with non-Gaussianity

Spherical Collapse Model

1. Spherical collapse model is a 1-1 mapping from the initial overdensity to the evolved nonlinear overdensity.

Spherical Collapse Model

1. Spherical collapse model is a 1-1 mapping from the initial overdensity to the evolved nonlinear overdensity.
2. It can be approximated by

$$\rho \equiv \frac{M}{\bar{\rho} V} = \left(1 - \frac{\delta_I}{\delta_c}\right)^{-\delta_c}, \tag{1}$$

where δ_I is the initial overdensity and $\delta_c = 1.66$ for ΛCDM universe.

Spherical Collapse Model

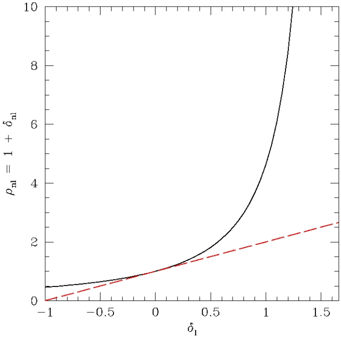

- $\rho_{nl} = 1 + \delta_{nl} \approx 1 + \delta_l$ when $\delta_l \sim 0$;

Spherical Collapse Model

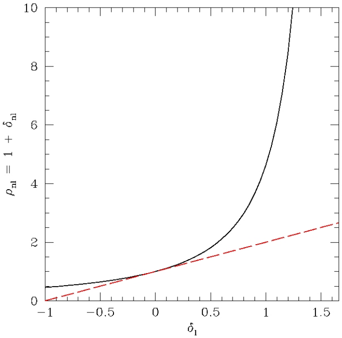

- $\rho_{nl} = 1 + \delta_{nl} \approx 1 + \delta_l$ when $\delta_l \sim 0$;
- ρ_{nl} diverges as $\delta_l \longrightarrow \delta_c$

Real Space PDF

3 assumptions:

1. A mapping from the initial overdensity δ_{L} to the evolved overdensity ρ

Real Space PDF

3 assumptions:

1. A mapping from the initial overdensity δ_{L} to the evolved overdensity ρ
2. ρ at any given position is determined only by the initial overdensity at the same location (in Lagrangian coordinate).

Real Space PDF

3 assumptions:

1. A mapping from the initial overdensity $\delta_{\rm L}$ to the evolved overdensity ρ
2. ρ at any given position is determined only by the initial overdensity at the same location (in Lagrangian coordinate).
3. The appropriate smoothing scale in the initial field is the scale whose mass M is associated with the evolved overdensity ρ.

Real Space PDF

3 assumptions:

1. A mapping from the initial overdensity $\delta_{\rm L}$ to the evolved overdensity ρ
2. ρ at any given position is determined only by the initial overdensity at the same location (in Lagrangian coordinate).
3. The appropriate smoothing scale in the initial field is the scale whose mass M is associated with the evolved overdensity ρ.

$$\int_{M}^{\infty} \mathrm{d}M' p(M'|V) \frac{M'}{\bar{M}} = \int_{\delta_L(M|V)/\sigma_L(M)}^{\infty} \mathrm{d}x \frac{\exp(-x^2/2)}{\sqrt{2\pi}}. \quad (2)$$

Real Space PDF

3 assumptions:

1. A mapping from the initial overdensity δ_{L} to the evolved overdensity ρ
2. ρ at any given position is determined only by the initial overdensity at the same location (in Lagrangian coordinate).
3. The appropriate smoothing scale in the initial field is the scale whose mass M is associated with the evolved overdensity ρ.

$$\int_{M}^{\infty} \mathrm{d}M' p(M'|V) \frac{M'}{\bar{M}} = \int_{\delta_L(M|V)/\sigma_L(M)}^{\infty} \mathrm{d}x \frac{\exp(-x^2/2)}{\sqrt{2\pi}}. \quad (2)$$

Extra weighting factor

Real space PDF using spherical collapse model

$$\rho^2 p(\rho|V) = \frac{1}{\sqrt{2\pi\sigma_L^2(\rho)}} \exp\left[-\frac{\delta_L^2(\rho)}{2\sigma_L^2(\rho)}\right]\left[1 - \frac{\delta_L(\rho)}{\delta_c} + \frac{\gamma}{6}\delta_L(\rho)\right], \tag{3}$$

where $\gamma = -3\mathrm{d}\ln\sigma_L^2/\mathrm{d}\ln M$.

Real space PDF

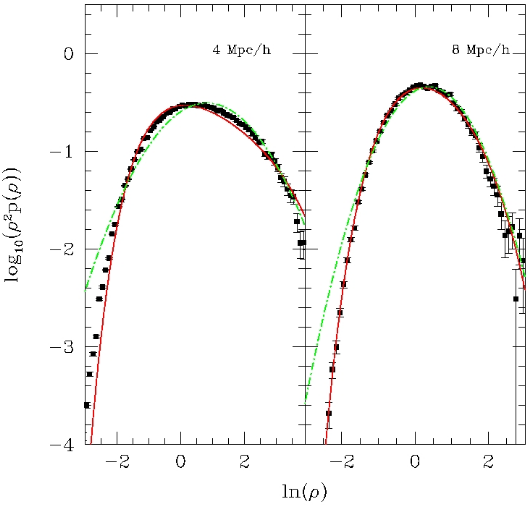

Outline

Introduction

Spherical Collapse and real space PDF

Ellipsoidal Collapse and zspace PDF

Large Scale Structure with non-Gaussianity

Ellipsoidal Collapse Model

1. The evolution of axes of a tri-axial object under gravity is governed by:

$$\frac{\mathrm{d}^2 R_k}{\mathrm{d}t^2} = H_0^2 \Omega_\Lambda R_k - 4\pi G \bar{\rho} R_k \left(\frac{1+\delta}{3} + \frac{b'_k}{2}\delta + \lambda'_{\mathrm{ext},k} \right), \quad (4)$$

(Bond & Myers 1996) where b'_k and $\lambda'_{\mathrm{ext},k}$ are the interior and exterior tidal forces respectively.

Ellipsoidal Collapse Model

1. The evolution of axes of a tri-axial object under gravity is governed by:

$$\frac{\mathrm{d}^2 R_k}{\mathrm{d}t^2} = H_0^2 \Omega_\Lambda R_k - 4\pi G \bar{\rho} R_k \left(\frac{1+\delta}{3} + \frac{b'_k}{2}\delta + \lambda'_{\mathrm{ext},k} \right), \quad (4)$$

   (Bond & Myers 1996) where b'_k and $\lambda'_{\mathrm{ext},k}$ are the interior and exterior tidal forces respectively.

2. Equation (4) has to be solved numerically in general. White & Silk (1979) and Shen et al. (2006) suggested an analytical approximation:

$$R_k(t) = \frac{a(t)}{a_i} R_k(t_i)[1 - D(t)\lambda_k] - \frac{a(t)}{a_i} R_h(t_i) \left[1 - \frac{D(t)}{3}\delta_i - \frac{a_e(t)}{a(t)} \right], \quad (5)$$

   where $R_h(t_i) = 3/\sum_j R_j(t_i)^{-1}$ and $a_e(t)$ is the expansion factor of a universe with initial overdensity $\delta_i = \sum_j \lambda_j(t_i)$.

Ellipsoidal Collapse Model: fitting formula

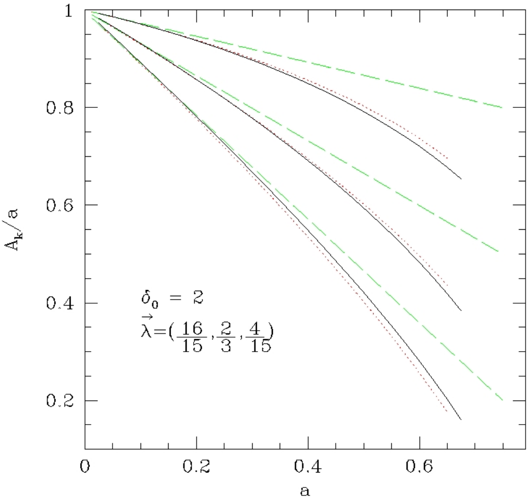

Modified Zeldovich Approximation

1. Zeldovich Approximation for overdensity:

$$\rho \equiv 1 + \delta = \prod_{j=1}^{3} \frac{1}{1 - D(t)\lambda_j.} \tag{6}$$

Modified Zeldovich Approximation

1. Zeldovich Approximation for overdensity:

$$\rho \equiv 1+\delta = \prod_{j=1}^{3} \frac{1}{1-D(t)\lambda_j.} \tag{6}$$

2. Modified approximation for overdensity from equation (5):

$$\rho = \frac{(1-D(t)\delta_i/3)^3}{(1-D(t)\delta_i/\delta_c)^{\delta_c}} \prod_{j=1}^{3} \frac{1}{1-D(t)\lambda_j}, \tag{7}$$

where $\delta_c \approx 1.66$. We approximate the scale factor $a_e(t)$ by the spherical collpase model.

Modified Zeldovich Approximation

1. Zeldovich Approximation for overdensity:

$$\rho \equiv 1 + \delta = \prod_{j=1}^{3} \frac{1}{1 - D(t)\lambda_j}. \tag{6}$$

2. Modified approximation for overdensity from equation (5):

$$\rho = \frac{(1 - D(t)\delta_i/3)^3}{(1 - D(t)\delta_i/\delta_c)^{\delta_c}} \prod_{j=1}^{3} \frac{1}{1 - D(t)\lambda_j}, \tag{7}$$

   where $\delta_c \approx 1.66$. We approximate the scale factor $a_e(t)$ by the spherical collpase model.

3. The correction term is the ratio of Zeldovich's prediction for the evolution of a sphere to the 'exact' evolution of a sphere.

Redshift space PDF

1. For any given ellipsoid, redshift-space to real-space overdensity is given by a mapping which depends on a velocity. This velocity is simply related to $\mathrm{d}R_k/\mathrm{d}t$ of the ellipsoid where R_k is from equation (5).

Redshift space PDF

1. For any given ellipsoid, redshift-space to real-space overdensity is given by a mapping which depends on a velocity. This velocity is simply related to $\mathrm{d}R_k/\mathrm{d}t$ of the ellipsoid where R_k is from equation (5).
2. We then account for the fact that the axes of the evolving ellipsoids are not pointing towards the observer, by defining the line-of-sight as being along the z-axis, and integrating over the Euler angles $(e_1, e_2, e_3) = (\cos\psi\sin\theta, \sin\psi\sin\theta, \cos\theta)$.

Redshift space PDF

1. For any given ellipsoid, redshift-space to real-space overdensity is given by a mapping which depends on a velocity. This velocity is simply related to $\mathrm{d}R_k/\mathrm{d}t$ of the ellipsoid where R_k is from equation (5).
2. We then account for the fact that the axes of the evolving ellipsoids are not pointing towards the observer, by defining the line-of-sight as being along the z-axis, and integrating over the Euler angles $(e_1, e_2, e_3) = (\cos\psi\sin\theta, \sin\psi\sin\theta, \cos\theta)$.

$$\rho_s\, p(\rho_s|V)\mathrm{d}\rho_s = \int \mathrm{d}\boldsymbol{\lambda}\mathrm{d}\mathbf{e}\, p(\boldsymbol{\lambda}|\sigma)\delta_{\mathrm{D}}\left[\rho_s = \rho_s'(\boldsymbol{\lambda}, \mathbf{e})\right], \tag{8}$$

Redshift space PDF

1. For any given ellipsoid, redshift-space to real-space overdensity is given by a mapping which depends on a velocity. This velocity is simply related to $\mathrm{d}R_k/\mathrm{d}t$ of the ellipsoid where R_k is from equation (5).
2. We then account for the fact that the axes of the evolving ellipsoids are not pointing towards the observer, by defining the line-of-sight as being along the z-axis, and integrating over the Euler angles $(e_1, e_2, e_3) = (\cos\psi \sin\theta, \sin\psi \sin\theta, \cos\theta)$.

$$\rho_s\, p(\rho_s|V)\mathrm{d}\rho_s = \int \mathrm{d}\boldsymbol{\lambda}\mathrm{d}\mathbf{e}\, p(\boldsymbol{\lambda}|\sigma)\delta_{\mathrm{D}}\left[\rho_s = \rho_s'(\boldsymbol{\lambda}, \mathbf{e})\right], \qquad (8)$$

Extra weighting factor

Redshift space PDF

8 $\mathrm{Mpc/h}$ Sphere

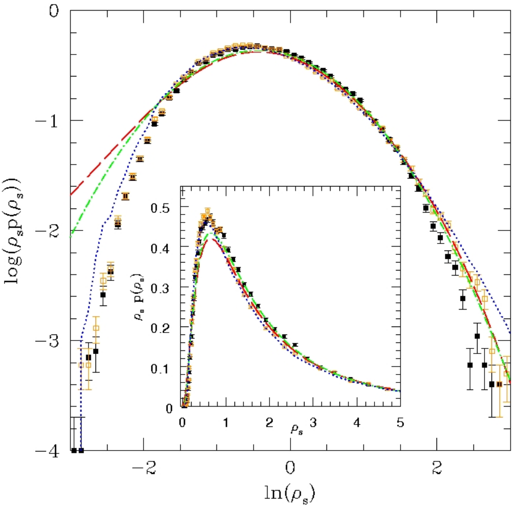

Redshift space PDF

4 Mpc/h Sphere

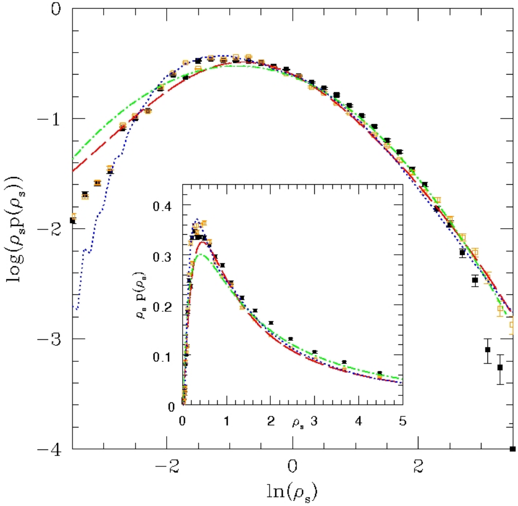

Outline

Introduction

Spherical Collapse and real space PDF

Ellipsoidal Collapse and zspace PDF

Large Scale Structure with non-Gaussianity

Large Scale Structure with non-Gaussianity

1. The computations of nonlinear PDF of dark matter field assume Gaussian initial conditions.

Large Scale Structure with non-Gaussianity

1. The computations of nonlinear PDF of dark matter field assume Gaussian initial conditions.
2. The collapse models and the statistical method are valid with non-Gaussian primordial perturbations.

Large Scale Structure with non-Gaussianity

1. The computations of nonlinear PDF of dark matter field assume Gaussian initial conditions.
2. The collapse models and the statistical method are valid with non-Gaussian primordial perturbations.
3. Large scale structure statistics I will look at for non-Gaussian primoridal perturbations:
    - Nonlinear probability distribution function of dark matter field
    - Distribution of shapes of void

1. Common parameterization of non-Gaussianity by f_{nl}:

$$\Phi = \phi + f_{nl}(\phi^2 - \langle\phi^2\rangle), \tag{9}$$

where Φ is the non-gaussian primordial perturbation potential, ϕ is the Gaussian primordial perturbation potential.

1. Common parameterization of non-Gaussianity by f_{nl}:

$$\Phi = \phi + f_{nl}(\phi^2 - \langle \phi^2 \rangle), \tag{9}$$

   where Φ is the non-gaussian primordial perturbation potential, ϕ is the Gaussian primordial perturbation potential.

2. CMB measurement on Gaussianity has different results on f_{nl}:
   - $-9 < f_{nl} < 111$ (WMAP 5-year; Komatsu et al. 2008)
   - $27 < f_{nl} < 147$ (WMAP 3-year; Yadav & Wandelt 2008)

1. Common parameterization of non-Gaussianity by f_{nl}:

$$\Phi = \phi + f_{nl}(\phi^2 - \langle\phi^2\rangle), \quad (9)$$

   where Φ is the non-gaussian primordial perturbation potential, ϕ is the Gaussian primordial perturbation potential.
2. CMB measurement on Gaussianity has different results on f_{nl}:
   - $-9 < f_{nl} < 111$ (WMAP 5-year; Komatsu et al. 2008)
   - $27 < f_{nl} < 147$ (WMAP 3-year; Yadav & Wandelt 2008)
3. Large scale structure on constraining f_{nl}:
   - Strong scale dependent of clustering of haloes in large scale (Dalal et al. 2008)
   - Slosar et al. (2008) obtained $-27 < f_{nl} < 70$ from SDSS luminous red galaxy and photometric quasar samples
   - Void abundance (Kamionkowski et al. 2008)
   - Probability distribution function of dark matter field from N-body simulation measurement (Grossi et al. 2008)

Nonlinear real space PDF with non-Gaussian initial conditions

Grossi et al. (2008)

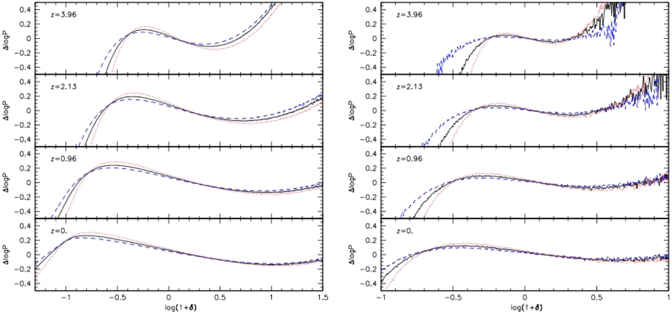

Figure 6. The logarithmic deviation of the PDF from a lognormal distribution, $\Delta \log P$, is shown for the same models and redshifts presented in Fig. 5. Results for smoothing radii $R_s \sim 0.98$ and $R_s \sim 3.91$ Mpc/h are displayed in the left and right panels, respectively. Different lines refer to models with different primordial non-Gaussianity: $f_{\rm NL} = 0$ (solid line), $f_{\rm NL} = 1000$ (dotted line), $f_{\rm NL} = -1000$ (dashed line).

Edgeworth Expansion

We will need the distributions of initial overdensity δ_I and the eigenvalues of the shear tensor $(\lambda_1, \lambda_2, \lambda_3)$. These distributions are approximated by the Edgeworth expansion:

$$p_{NG}(x|V)\ dx = \frac{e^{-\nu^2/2}}{\sqrt{2\pi}} \left[1 + \frac{\sigma_x S_3}{6} H_3(\nu) + \ldots\right]\ d\nu, \tag{10}$$

where $\sigma_x^2 = \langle x^2 \rangle$ is the variance of x, $S_3 = \langle x^3 \rangle / \sigma_x^4 = \gamma_x^3 / \sigma_x^4$, $\nu = x/\sigma_x$, and $H_3(\nu) = \nu^3 - 3\nu$. Note that there is an implicit smoothing scale in σ_x and γ_x^3 of equation (10).

$S_3(r)$ and $\sigma(r)S_3(r)$

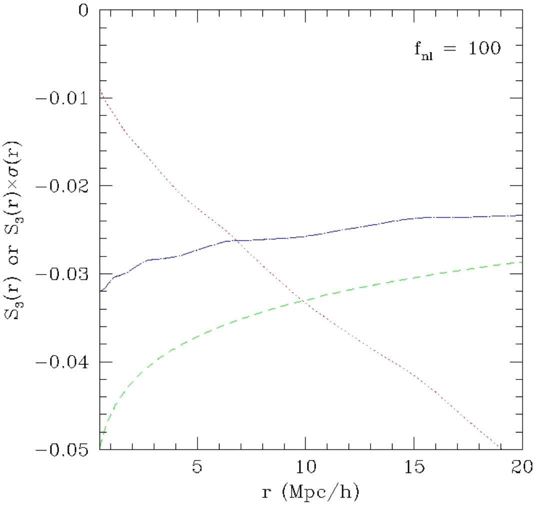

Edgeworth expansion and initial distributions

$\lambda_1, \lambda_2, \lambda_3$

Edgeworth expansion and initial distributions

$\lambda_1, \lambda_2, \lambda_3$

1. Apply Edgeworth expansion on the set of six independent variables $\{x, y, z, \Phi_{12}, \Phi_{23}, \Phi_{31}\}$ where:

$$
\begin{aligned}
x &= \sum_i \Phi_{ii} \\
y &= \frac{1}{2}(\Phi_{11} - \Phi_{22}) \\
z &= \frac{1}{2}(\Phi_{11} + \Phi_{22} - 2\Phi_{33})
\end{aligned}
$$

Edgeworth expansion and initial distributions

$\lambda_1, \lambda_2, \lambda_3$

1. Apply Edgeworth expansion on the set of six independent variables $\{x, y, z, \Phi_{12}, \Phi_{23}, \Phi_{31}\}$ where:

$$
\begin{aligned}
x &= \sum_i \Phi_{ii} \\
y &= \frac{1}{2}(\Phi_{11} - \Phi_{22}) \\
z &= \frac{1}{2}(\Phi_{11} + \Phi_{22} - 2\Phi_{33})
\end{aligned}
$$

2. Then find $(\lambda_1, \lambda_2, \lambda_3)$ by solving the eigenvalue equations.

Initial Distributions with non-Gaussian initial conditions

$f_{nl} = \pm 100$

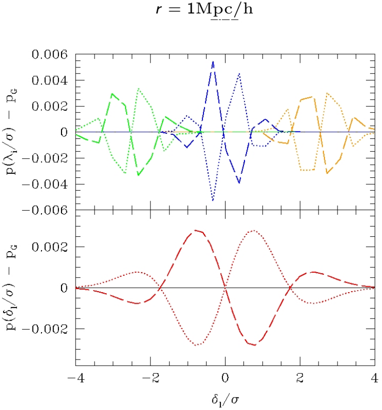

Initial Distributions: ellipicity and prolateness

Define ellipiticity e and prolateness p:

$$e = \frac{\lambda_1 - \lambda_3}{2\delta_l}, \text{ and } p = \frac{\lambda_1 + \lambda_3 - 2\lambda_2}{2\delta_l} \tag{11}$$

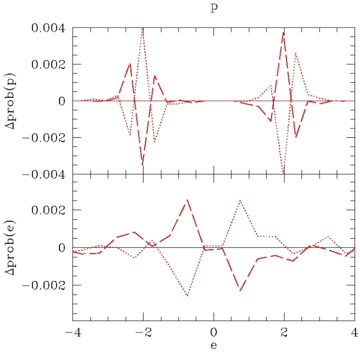

$r = 1\mathrm{Mpc/h}$

Nonlinear real space PDF with non-Gaussian initial conditions

1. Same spherical collapse model:

$$\rho = \left(1 - \frac{\delta_l}{\delta_c}\right)^{-\delta_c}, \tag{12}$$

Nonlinear real space PDF with non-Gaussian initial conditions

1. Same spherical collapse model:

$$\rho = \left(1 - \frac{\delta_l}{\delta_c}\right)^{-\delta_c}, \tag{12}$$

2. Nonlinear PDF:

$$\rho^2 p(\rho|V) = \frac{1}{\sqrt{2\pi\sigma^2(\rho)}} \exp\left[-\frac{\delta_l^2(\rho)}{2\sigma^2(\rho)}\right] \left[1 - \frac{\delta_l(\rho)}{\delta_c} + \frac{\gamma_\sigma}{6}\delta_l(\rho)\right] \times \left[1 + \frac{\sigma(\rho)S_3(\rho)}{6} H_3\left(\frac{\delta_l(\rho)}{\sigma(\rho)}\right)\right]. \tag{13}$$

Real space PDF with non-Gaussian initial conditions

r =4Mpc/h

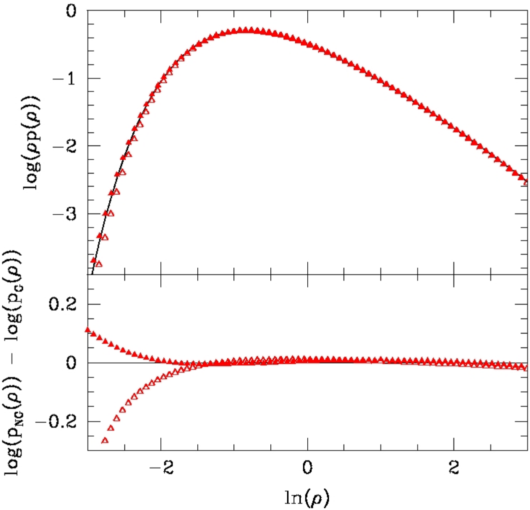

r =8Mpc/h

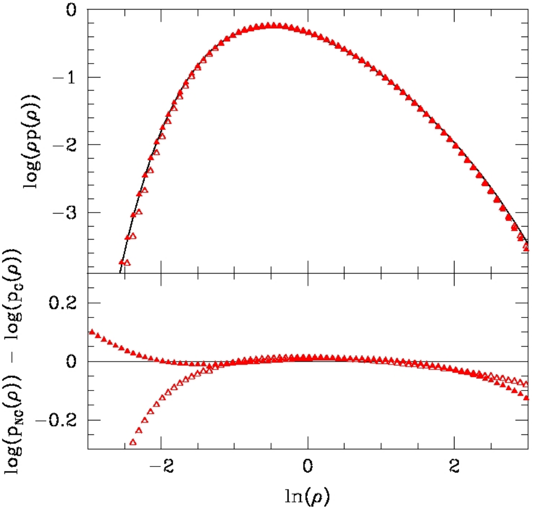

Nonlinear PDF with non-Gaussian initial conditions

Results

1. Non-Gaussian initial conditions slightly modify the nonlinear PDF.

Nonlinear PDF with non-Gaussian initial conditions

Results

1. Non-Gaussian initial conditions slightly modify the nonlinear PDF.
2. The modification shows up in underdense regions.

Nonlinear PDF with non-Gaussian initial conditions

Results

1. Non-Gaussian initial conditions slightly modify the nonlinear PDF.
2. The modification shows up in underdense regions.
3. Our analytical calculation matches qualitatively with the measurements from numerical simulation in the literature.

Shape of Voids

Approximation of axis ratio by Ellipsoidal Collapse Model

1. We approximate the evolution of axis by the ellipsoidal collapse model;

Shape of Voids

Approximation of axis ratio by Ellipsoidal Collapse Model

1. We approximate the evolution of axis by the ellipsoidal collapse model;
2. This approximation is based on Shen et al. (2006):

$$R_k = R_k^i(1 - \lambda_k) - R_2^i(1 - \lambda_2)\left[1 - \frac{(1 - \delta_l/\delta_c)^{\delta_c/3}}{1 - \delta_l/3}\right], \quad (14)$$

where R_k^i is the initial axis i.

Shape of Voids

Approximation of axis ratio by Ellipsoidal Collapse Model

1. We approximate the evolution of axis by the ellipsoidal collapse model;
2. This approximation is based on Shen et al. (2006):

$$R_k = R_k^i(1-\lambda_k) - R_2^i(1-\lambda_2)\left[1 - \frac{(1-\delta_I/\delta_c)^{\delta_c/3}}{1-\delta_I/3}\right], \quad (14)$$

   where R_k^i is the initial axis i.
3. We will look at the distribution of shapes of voids with initial smoothing scale $= 1\, h^{-1}\mathrm{Mpc}$.

Distribution of R_1/R_3

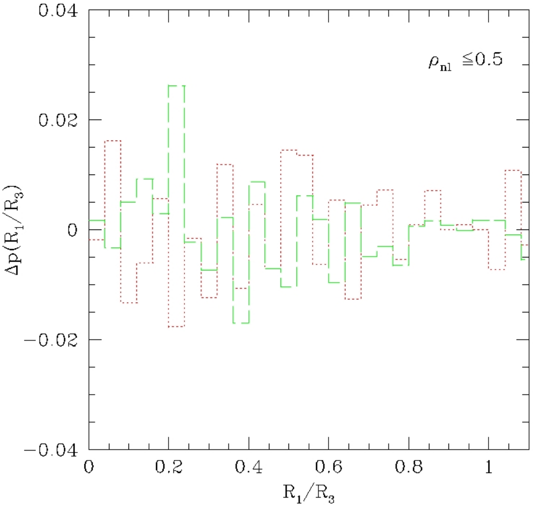

Distribution of R_2/R_3

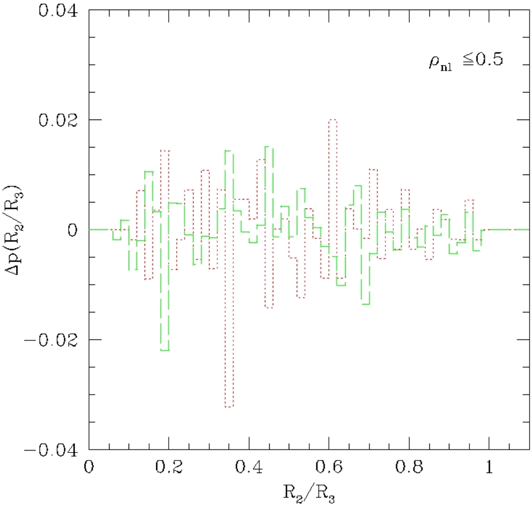

Shape of voids with non-Gaussian initial conditions

Result

1. The distribution of axis ratio changes and the difference is in the percent level.

Shape of voids with non-Gaussian initial conditions

Result

1. The distribution of axis ratio changes and the difference is in the percent level.
2. Measurements of shape of voids from numerical simulation with Gaussian initial conditions (Park & Lee 2007):

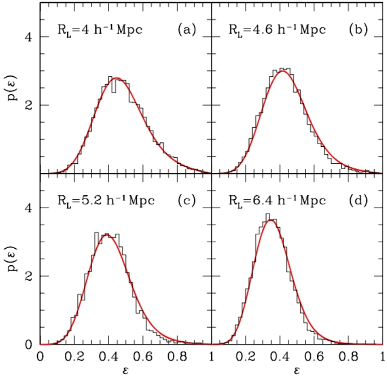

Conclusion/Discussion

1. Primordial non-Gaussian perturbation modifies the statistics of large scale structure.

Conclusion/Discussion

1. Primordial non-Gaussian perturbation modifies the statistics of large scale structure.
2. The non-gaussian signal in nonlinear PDF shows up in underdense region.

Conclusion/Discussion

1. Primordial non-Gaussian perturbation modifies the statistics of large scale structure.
2. The non-gaussian signal in nonlinear PDF shows up in underdense region.
3. For a reasonable value of f_{nl}, the change in the nonlinear PDF is small.

Conclusion/Discussion

1. Primordial non-Gaussian perturbation modifies the statistics of large scale structure.
2. The non-gaussian signal in nonlinear PDF shows up in underdense region.
3. For a reasonable value of f_{nl}, the change in the nonlinear PDF is small.
4. Non-gaussian signal differentiates from the Gaussian one in the distribution of shape of voids.

Conclusion/Discussion

1. Primordial non-Gaussian perturbation modifies the statistics of large scale structure.
2. The non-gaussian signal in nonlinear PDF shows up in underdense region.
3. For a reasonable value of f_{nl}, the change in the nonlinear PDF is small.
4. Non-gaussian signal differentiates from the Gaussian one in the distribution of shape of voids.
5. For a full analysis of distribution of shape of voids, one has to include different initial smoothing scales and shapes, as well as taking into account the effects of void-in-void and void-in-cloud.

END

Reconstruction of initial distribution

1. Spherical collapse model (1-1 mapping) allows a reconstruction of the initial distribution from the measured nonlinear density field;

Reconstruction of initial distribution

1. Spherical collapse model (1-1 mapping) allows a reconstruction of the initial distribution from the measured nonlinear density field;
2. For each measured δ_{nl}:

$$\nu = \frac{1 - [(1+\delta_{NL})/N_{sc}]^{-1/\delta_c}}{\sigma_L(M/N_{sc})/\delta_c}. \tag{15}$$

Reconstruction of initial distribution

1. Spherical collapse model (1-1 mapping) allows a reconstruction of the initial distribution from the measured nonlinear density field;
2. For each measured δ_{nl}:

$$\nu = \frac{1 - [(1+\delta_{NL})/N_{sc}]^{-1/\delta_c}}{\sigma_L(M/N_{sc})/\delta_c}. \tag{15}$$

3. Make a histogram of ν, weight each cell by its value $(1+\delta_{nl})/N_{sc}$

Reconstruction of initial distribution (real space)

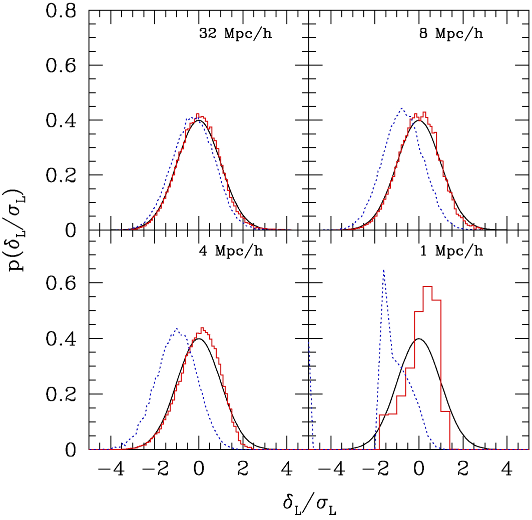

Reconstruction of initial distribution in redshift space

1. In redshift space nonlinear PDF calculation, the ellipsoidal collapse model (3-1 mapping) complicates the reconstruction;

Reconstruction of initial distribution in redshift space

1. In redshift space nonlinear PDF calculation, the ellipsoidal collapse model (3-1 mapping) complicates the reconstruction;
2. Apply empirial relation found in Scherrer & Gaztañaga (2001):

$$p(\nu_r)d\nu_r = p(\nu_s)d\nu_s, \text{ and } \nu_r = \nu_s, \tag{16}$$

This implies $\delta_s = \delta_r(\sigma_s/\sigma_r)$.

Reconstruction of initial distribution in redshift space

1. In redshift space nonlinear PDF calculation, the ellipsoidal collapse model (3-1 mapping) complicates the reconstruction;
2. Apply empirial relation found in Scherrer & Gaztañaga (2001):

   $$p(\nu_r)d\nu_r = p(\nu_s)d\nu_s, \text{ and } \nu_r = \nu_s, \tag{16}$$

   This implies $\delta_s = \delta_r(\sigma_s/\sigma_r)$.
3. Using the Kaiser formula and the real-space reconstruction method (equation 15).

Reconstruction of initial distribution (redshift space)

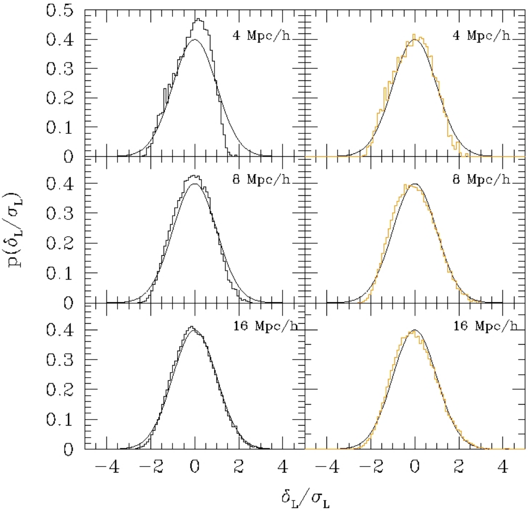

Application of reconstruction method

Reconstruction of the BAO signal (Eisenstein et al. 2006):

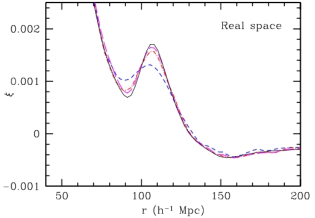

FIG. 3.— The real-space matter correlation function after reconstruction by the linear-theory density-velocity relation, with the density field Gaussian filtered. The black solid line shows the correlation function at $z = 49$. The blue short-dashed line shows it at $z = 0.3$; the acoustic peak has been smeared out. The red dot-dashed and magenta long-dashed lines show the effects of reconstruction for $20h^{-1}$ Mpc and $10h^{-1}$ Mpc Gaussian filtering, respectively. Even this very simple reconstruction recovers nearly all of the linear acoustic peak.

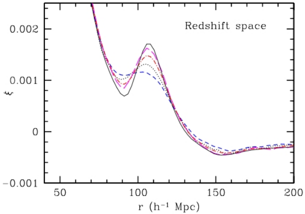

FIG. 4.— The redshift-space matter correlation function after reconstruction by the linear-theory density-velocity relation, with the density field Gaussian filtered. The black solid line shows the correlation function at $z = 49$. The blue short-dashed line shows the redshift-space correlation function at $z = 0.3$; the acoustic peak has been smeared out. The black dotted line shows the real-space correlation function for comparison. The red dot-dashed line line shows the effects of reconstruction for a $10h^{-1}$ Mpc Gaussian filtering; the magenta long-dashed line is the result when one compresses the fingers of God prior to the reconstruction. These reconstructions significantly improve the acoustic peak.